Available online at www.sciencedirect.com
ScienceDirect
Ceramics International 37 (2011) 2391–2396
CERAMICS INTERNATIONAL
www.elsevier.com/locate/ceramint

Annealing-induced changes in the nanoscale electrical homogeneity of bismuth ferrite dielectric thin films

Yuan-Chang Liang *, W.S. Chen, Chia-Yen Hu, Chiem-Lum Huang, W. Kai

Institute of Materials Engineering, National Taiwan Ocean University, Keelung 20224, Taiwan

Received 28 January 2011; received in revised form 18 March 2011; accepted 21 March 2011
Available online 29 March 2011

Abstract

In this study, we investigated the effects of forming gas (7% H_2 + 93% Ar) annealing (FGA) and recovery annealing (RA) in ambient oxygen on the structure and electrical properties of $BiFeO_3$ (BFO) thin films. X-ray diffraction results indicate that BFO remains in the perovskite phase following FGA. However, the spatial distribution of current maps obtained by conductive atomic force microscopy shows that FGA-treated BFO thin films are less electrically insulating than those without prepared thermal annealing. Recovery annealing improves the structural and chemical homogeneity of the FGA-treated films, thereby increasing the electrical resistance of the films.

Keywords: A. Films; B. Defects; B. Surfaces; C. Electrical properties; D. Perovskites

1. Introduction

Bismuth ferrite thin films have been widely investigated due to their multiferroic properties and potential applications in a wide range of novel devices [1,2]. Recently, numerous works have reported the structural and physical properties of bismuth ferrite thin films integrated with Si substrates in Si-based devices [3,4]. Although a great deal of effort has gone into improving the physical properties of bismuth ferrite thin films to allow fabrication of devices with high reliability, the high levels of leakage current of bismuth ferrite in the form of a thin film structure remain a major drawback limiting the application of such thin films in memory devices. Considerable effort has gone into developing methods for the deposition of bismuth ferrite thin films, including pulsed laser deposition, chemical solution deposition, and sputtering [1,3,5–7]. Many factors related to structural and/or chemical defects in the material have been proposed to affect the electrical properties of bismuth thin films [1,3].

Forming gas annealing (FGA) can be used for the integration of bismuth ferrite thin films in Si-based devices. This process is adopted to neutralize the possibility of trapping charges that are generated during the preparation of the oxide heterostructure at the Si/SiO_2 interface. Several works have shown that such an annealing markedly reduces the electrical properties of ferroelectric or dielectric oxide thin films [8,9]. The electrical properties of bismuth ferrite thin films are largely dependent on the process parameters and techniques involved in their synthesis, and the thermal annealing procedures of bismuth ferrite thin films during fabrication are critical to the reliability of the devices. However, only a limited number of studies have been conducted on the effects of FGA with regard to the structural and electrical properties of bismuth ferrite thin films. Moreover, to improve the electrical properties of bismuth ferrite thin films in nanodevice applications, it is necessary to understand the correlation between material defect and the spatial distribution of the current maps of bismuth ferrite thin films treated with FGA. This work investigated the effects of FGA on the characteristics of bismuth ferrite thin films. Moreover, we performed recovery annealing (RA) in ambient oxygen at the same temperature as FGA to determine the degree of recovery of the physical properties of the FGA-treated bismuth ferrite thin films.

2. Experimental

Eighty-nanometer-thick $BiFeO_3$ (BFO) thin films were grown on Pt (150 nm)/Ti/SiO_2/Si (1 0 0) substrates with and without the 100 nm-thick LNO buffer. Thin film deposition was

* Corresponding author. Tel.: +886 2 24622192; fax: +886 2 24625324.
E-mail addresses: yuanvictory@gmail.com, dean1818@gmail.com (Y.-C. Liang).

0272-8842/$36.00
doi:10.1016/j.ceramint.2011.03.029

performed using a radio-frequency magnetron sputtering system. During deposition of the BFO thin films, the substrate temperature was kept at 350 °C, and the gas pressure of deposition was fixed at 15 mTorr with an Ar/O_2 ratio of 4:1. The LNO bottom electrode was prepared at 500 °C, and the gas pressure was 30 mTorr with an Ar/O_2 ratio of 4:1 [10]. Some of the BFO thin films were subsequently annealed in a rapid thermal annealing furnace with 300 Torr forming gas (7% H_2 + 93% Ar) at 400 °C for 20 min. The recovery annealing was performed in an oxygen atmosphere (300 Torr) at 400 °C for 40 min for the FGA-treated samples.

The crystallographic structures of the BFO thin films were analyzed by X-ray diffraction (XRD) with Cu Kα radiation. The composition depth profile was examined with secondary ion mass spectrometry (SIMS). The surface morphology of the BFO thin films was investigated with atomic force microscopy (AFM). The chemical bonding states of the constituent elements of BFO thin films were determined using X-ray photoelectron spectroscopy (XPS). The surface current images of the BFO thin films were observed by conductive atomic force microscope (CAFM) with PtIr tips under a bias voltage of 4 V.

3. Results and discussion

Fig. 1(a) shows that BFO thin films grown on $Pt/Ti/SiO_2/Si$ (1 0 0) substrates (BFO/Pt) were polycrystalline with random crystallographic features. Differences in the crystal structure and chemical properties between BFO and Pt lead to the growth of BFO thin films with a random crystallographic orientation on the Pt. In contrast, BFO thin films grown on LNO-buffered $Pt/Ti/SiO_2/Si$ (1 0 0) substrates (BFO/LNO) showed a satisfactory (*h* 0 0)-oriented crystallographic structure (Fig. 1(b)). XRD patterns show that the BFO/Pt and BFO/LNO thin films retained their perovskite structure after FGA at 400 °C for 20 min. No impurity phase was detected in the XRD patterns of the BFO/Pt or BFO/LNO thin films treated with thermal annealing. However, the intensity of the Bragg reflections of the BFO thin films decreased after FGA. This decrease could be associated with the fact that the films become more microstructurally heterogeneous following FGA. Subsequent recovery annealing improved the intensity of the Bragg reflections of FGA-treated BFO thin films; however, the peak intensities were still lower than those of as-deposited BFO films.

Fig. 2 shows the measurements of SIMS for the BFO/Pt and BFO/LNO thin films treated with FGA at 400 °C. A large number of hydrogen atoms were present in the FGA-treated BFO/Pt and BFO/LNO thin films. The diffusion of hydrogen into dielectric oxide films following FGA at high temperatures has been identified by SIMS depth profiling [8,11]. The observation of the H signal in the SIMS spectra for the BFO/Pt and BFO/LNO thin films prepared by FGA at 400 °C is in agreement with previous studies. Hydrogen ions could lead to a reduction of bismuth oxide. Moreover, hydrogen in the lattice of the BFO or at the grain boundaries in the films resulting from FGA at 400 °C may lead to deterioration in the quality of the crystals in BFO/Pt and BFO/LNO thin films, further influencing the electrical properties of the films. It has been

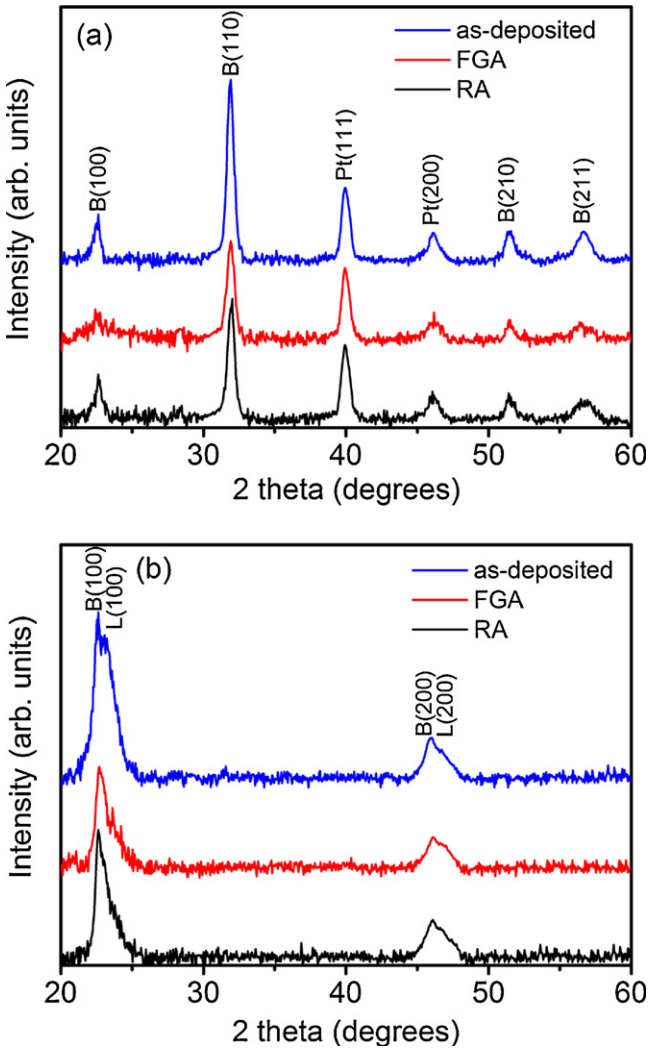

Fig. 1. (a) XRD patterns of the BFO/Pt thin films without and with thermal annealing at 400 °C. (b) BFO/LNO thin films with and without thermal annealing at 400 °C. FGA and RA denote forming gas annealing and recovery annealing in ambient oxygen, respectively.

reported that, following FGA, exposure to a reducing atmosphere increases the number of oxygen vacancies, leading to a reduction at the grain boundaries in polycrystalline dielectric oxide films [12].

Fig. 3 shows narrow scans of the XPS spectra of BFO/Pt thin films following thermal annealing. The bismuth and iron ions of the as-deposited films were in a trivalent oxidation state (data not shown). The Bi 4f orbital of the BFO thin films prepared by FGA and recovery annealing at 400 °C (Fig. 3(a and b)) shows that bismuth ions were not in the trivalent oxidation state. Fig. 3(a and b) shows the doublet of the oxidized Bi^{+3} 4f core level together with that of the Bi^0 4f core level for BFO thin films treated with FGA and recovery annealing. The metallic Bi^0 4f core level may be formed by the reduction of Bi^{+3} in the reducing atmosphere. The reduction of bismuth oxide to metallic bismuth was observed after thermal annealing in ambient hydrogen [13]. The area ratio of metallic Bi to Bi^{+3} at the core level was comparatively larger for FGA-treated BFO

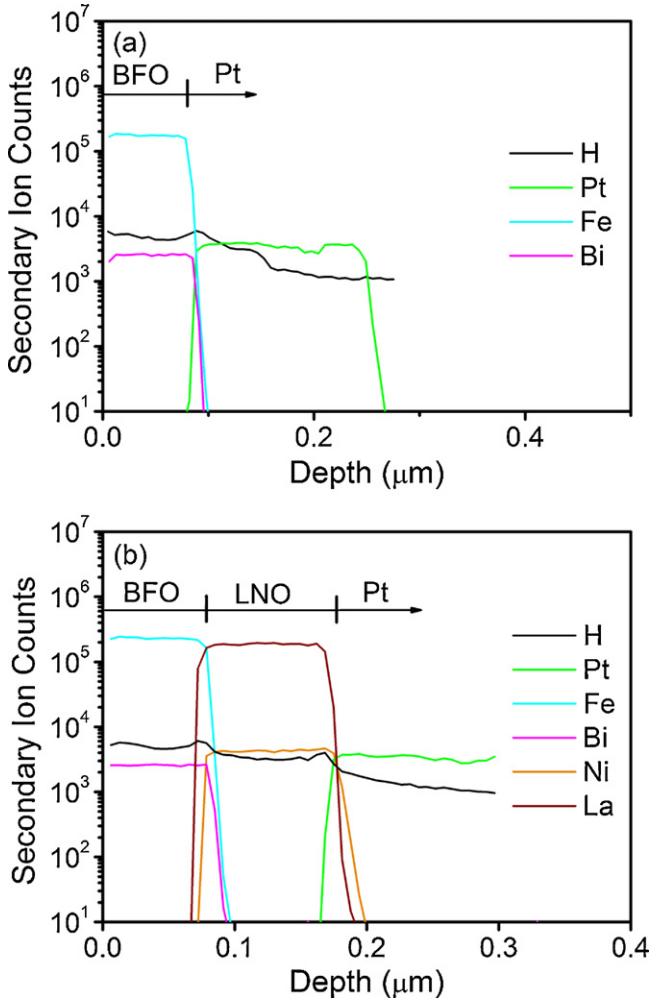

Fig. 2. SIMS depth profiles of the BFO/Pt and BFO/LNO thin films prepared by FGA at 400 °C: (a) BFO/Pt and (b) BFO/LNO.

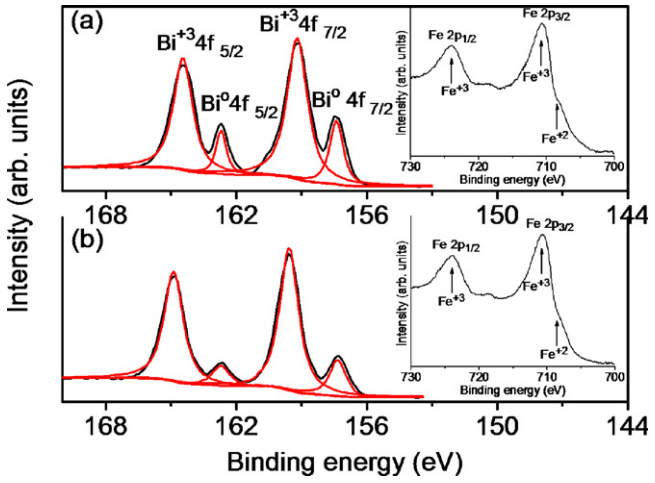

Fig. 3. High-resolution XPS spectra of Bi 4f core levels of BFO thin films: (a) FGA at 400 °C and (b) recovery annealing at 400 °C. The Fe 2p spectra are shown in the insets. The arrows located at ~708.5 eV correspond to Fe^{+2}.

thin films than for recovery annealed films, showing a difference in energy between the Bi^{+3} 4f doublet and the metallic 4f doublet for the BFO thin film, with the ration for the FGA films notably lower than that of the recovery annealed films (~1.76 eV for FGA-treated films and 2.32 eV for the RA-treated films). The Bi–O bonds were broken by FGA but could be recovered through the reaction of Bi and O in ambient oxygen during oxygen recovery annealing [14]. A high-temperature recovery annealing process (700–800 °C) was adopted to repair chemical defects in $SrBi_2Ta_2O_9$ oxide thin films following FGA treatment [15]. The chemical configuration of iron ions in BFO thin films following thermal annealing was a mixed-valence state. The origin of Fe^{+2} ions might be associated with changes in the valance of Bi and/or the occurrence of oxygen vacancies in the films following thermal annealing [16,17]. XPS results reveal that FGA caused a reduction in Bi^{+3} and the formation of oxygen vacancies in the BFO thin films. Subsequent recovery annealing improved the chemical homogeneity of the FGA-treated films.

Fig. 4 shows the surface topography of the BFO thin films with and without thermal treatment. The surface of as-deposited BFO/LNO thin films was smoother and denser than that of the as-deposited BFO/Pt thin films (Fig. 4(a and d)). The root-mean-square (RMS) surface roughnesses of the BFO/Pt and BFO/LNO thin films without thermal annealing were ~4.31 and 2.3 nm, respectively. The LNO buffer layer reduced the surface roughness of the BFO thin films. Moreover, the surface topography of the BFO/Pt and BFO/LNO thin films was not markedly changed by thermal annealing, perhaps because the temperature of FGA and recovery annealing (400 °C) was slightly higher than the temperature during the growth of the BFO thin films. The annealing temperature was inadequate to provide the driving force required to cause a transformation in the topography of the thin films. The FGA slightly roughened the surface of the film from 4.31 to 5.36 nm and from 2.3 to 2.75 nm for BFO/Pt and BFO/LNO films, respectively. Moreover, the subsequent recovery annealing in an oxygen atmosphere did not reduce the surface roughness of the films (the RMS roughnesses of the RA-treated BFO/Pt and BFO/LNO films were 5.43 and 2.79 nm, respectively.) The relatively rough surface of the film resulting from FGA was more likely to cause nanoscale electrical inhomogeneity in the dielectric oxide films [18].

Fig. 5 shows the current maps for the BFO/Pt and BFO/LNO thin films with and without thermal annealing measured at an applied bias of 4 V during AFM scanning. The color of the current maps of the as-deposited BFO/Pt and BFO/LNO thin films was dark, revealing that the films remained highly electrically resistant under an applied voltage of 4 V, corresponding to an average electric field of 500 kV/cm. Furthermore, the FGA-treated BFO/Pt and BFO/LNO thin films showed a large number of spots (white regions) of high current leakage over the area of interest. Hydrogen atoms diffuse into the BFO films during FGA, causing a reduction in Bi^{+3} in the BFO thin films, and accumulation of hydrogen at the grain boundaries of the BFO thin films is associated with FGA at 400 °C. The poor electrical resistance of the dielectric oxide thin films is attributable to these factors. Recent work has suggested that defects and impurity energy levels in the band

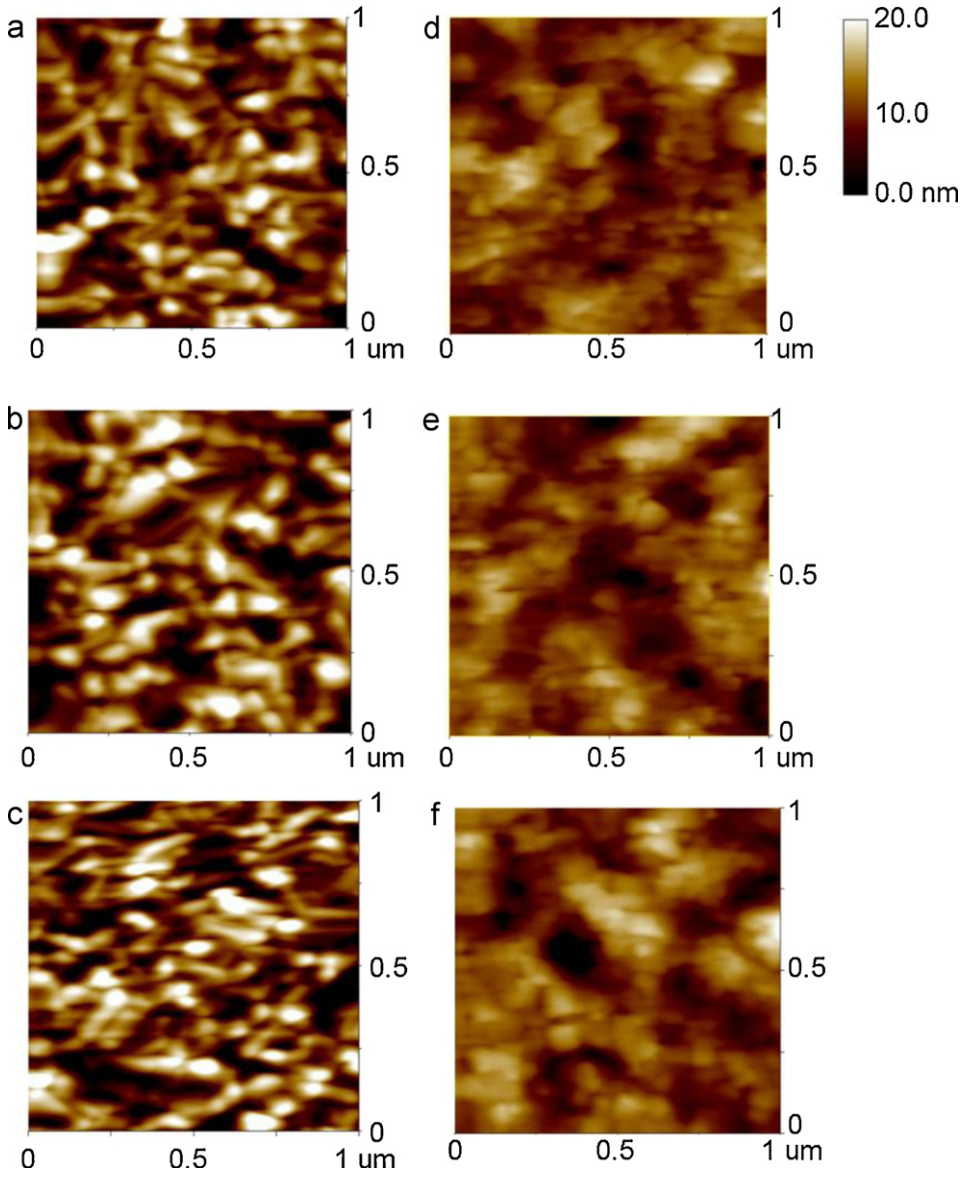

Fig. 4. AFM surface images of the BFO/Pt and BFO/LNO thin films: (a) as-deposited BFO/Pt, (b) BFO/Pt with FGA at 400 °C, (c) BFO/Pt with recovery annealing at 400 °C, (d) as-deposited BFO/LNO, (e) BFO/LNO with FGA at 400 °C, and (f) BFO/LNO with recovery annealing at 400 °C.

gap can lead to high leakage currents [19]. FGA causes a large increase in current leakage in perovskite $SrTiO_3$ films [20]. It is been suggested that interstitial hydrogen acts as a shallow donor in dielectric $SrTiO_3$, contributing to the conductivity of the oxide [21]. Moreover, oxygen vacancies have been verified as the main cause of high current leakage in BFO thin films [22]. BFO/Pt thin films had a higher level of electrical leakage than BFO/LNO thin films under the same FGA conditions, indicating that the relatively rough surface topography of BFO/Pt thin films results in worse structural inhomogeneity in the film when treated with FGA. In contrast, the subsequent recovery annealing of FGA-treated BFO/Pt and BFO/LNO thin films in ambient oxygen markedly recovered the nanoscale leakage characteristics of the films, as shown in Fig. 5. The highly conductive regions of BFO/Pt and BFO/LNO thin films were largely reduced following RA, compared to those of FGA-treated thin films. Although the duration of recovery annealing was double that of FGA, the recovery annealed BFO/Pt and BFO/LNO thin films were not electrically insulating, with an electric field strength of 500 kV/cm. This observation is consistent with previous studies and has been associated with the fact that oxygen-recovery annealing may eliminate the negative effects of incorporating hydrogen in the oxide; however, many oxygen vacancies remain in the crystal following recovery annealing, reducing the electrical resistance of the dielectric films. A comparison of the current maps between recovery annealed BFO/Pt and BFO/LNO thin films demonstrated that the BFO film grown without an LNO buffer had worse leakage characteristics than films grown with an LNO buffer. This result reveals that the homogeneity in the surface of the original film also influences the nanoscale electrical properties of annealed BFO thin films.

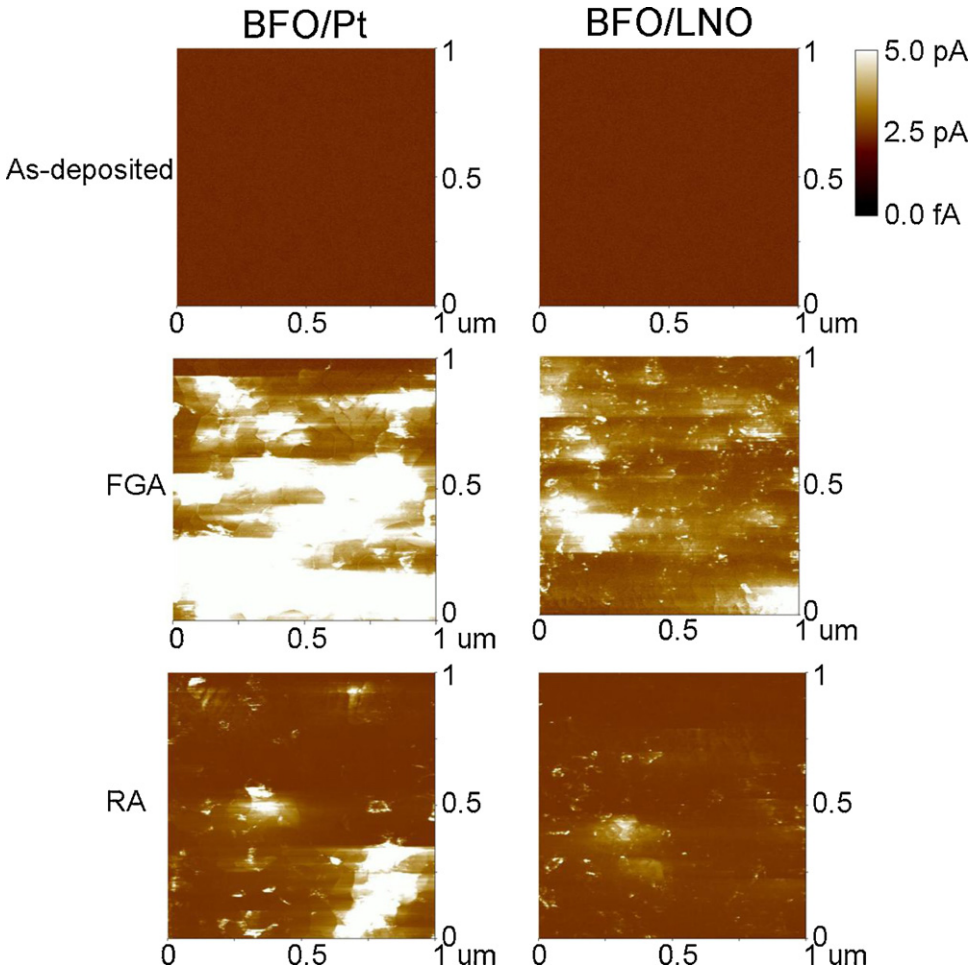

Fig. 5. The current maps of the BFO/Pt and BFO/LNO thin films with and without thermal annealing. The current maps were obtained under the bias voltage of 4 V during AFM measurements.

4. Conclusions

The diffusion of hydrogen into BFO oxide films treated with FGA at 400 °C was identified using SIMS depth profiling. A marked reduction of Bi^{+3} in the BFO thin film was observed following FGA at 400 °C. Moreover, the subsequent recovery annealing of FGA-treated BFO thin films in ambient oxygen led to an improvement in the chemical homogeneity of the films. A reduction of Bi^{+3} in the film and hydrogen in the oxide lattice in conjunction with the possible accumulation of grain boundaries might account for the poor electric insulating properties of FGA-treated BFO thin films. The leakage current of FGA-treated films largely decreased following recovery annealing at 400 °C in ambient oxygen, although the films were not as electrically insulating as as-deposited films.

Acknowledgments

This work was financially supported by the National Science Council of the Republic of China (grant no. NSC 99-2221-E-019-055) and the National Taiwan Ocean University (grant no. NTOU-RD-AA-2010-104031).

References

[1] Y.C. Liang, Y.C. Liang, "Enhancement of nanoscale leakage current performance of bismuth ferrite thin films using conductive oxide electrodes", J. Electrochem. Soc. 156 (2009) G84–G87.
[2] M. Bibes, A. Barthélémy, Multiferroics: towards a magnetoelectric memory, Nat. Mater. 7 (2008) 425–426.
[3] Y.H. Lee, J.M. Wu, Y.L. Chueh, L.J. Chou, Low-temperature growth and interface characterization of $BiFeO_3$ thin films with reduced leakage current, Appl. Phys. Lett. 87 (2005) 172901–172903.
[4] S.K. Singh, R. Ueno, H. Funakubo, H. Uchida, S. Koda, H. Ishiwara, Dependence of ferroelectric properties on thickness of $BiFeO_3$ thin films fabricated by chemical solution deposition, Jpn. J. Appl. Phys. 44 (2005) 8525–8527.
[5] Y. Wang, C.W. Nan, Integration of $BiFeO_3$ thin films on Si wafer via a simple sol–gel method, Thin Solid Films 517 (2009) 4484–4487.
[6] C. Ternon, J. Thery, T. Baron, C. Ducros, F. Sanchette, J. Kreisel, Structural properties of films grown by magnetron sputtering of a $BiFeO_3$ target, Thin Solid Films 515 (2006) 481–484.
[7] S.R. Das, P. Bhattacharya, R.N.P. Choudhary, R.S. Katiyar, Effect of La substitution on structural and electrical properties of $BiFeO_3$ thin film, J. Appl. Phys. 99 (2006) 066107–066109.
[8] Y.C. Liang, Hydrogen-induced degradation in physical properties of dielectric-enhanced $Ba_{0.6}Sr_{0.4}TiO_3/SrTiO_3$ artificial superlattices, Electrochem. Solid State Lett. 13 (2010) G91–G94.

[9] U. Chon, K.B. Kim, H.M. Jang, Degradation mechanism of ferroelectric properties in Pt/$Bi_{4-x}La_xTi_3O_{12}$/Pt capacitors during forming gas annealing, Appl. Phys. Lett. 79 (2001) 2450–2452.

[10] Y.C. Liang, Crystallographic effects on nanoscale electrical properties of ultrathin lanthanum aluminate films, Electrochem. Solid State Lett. 12 (2009) G57–G60.

[11] B.C. Lan, J.J. Hsu, S.Y. Chen, J.S. Bow, Forming gas annealing on physical characteristics and electrical properties of $Sr_{0.8}Bi_2Ta_2O_9$/Al_2O_3/Si capacitors, J. Appl. Phys. 94 (2003) 1877–1881.

[12] N. Cramer, A. Mahmud, T.S. Kalkur, Effect of annealing on leakage current in $Ba_{0.5}Sr_{0.5}TiO_3$ and $Ba_{0.96}Ca_{0.04}Ti_{0.84}Zr_{0.16}O_3$ thin films with Pt electrodes, Appl. Phys. Lett. 87 (2005) 032903–032905.

[13] I. Koiwa, T. Kanehara, H. Kato, S. Ono, A. Sakakibara, T. Osaka, K. Asami, Effects of H_2 sintering and Pt upper electrode on metallic Bi content in $Sr_{0.9}Bi_{2.1}Ta_2O_9$ thin films for ferroelectric memories prepared by sol–gel method, Jpn. J. Appl. Phys. 1 (37) (1998) 5192–5197 (part 1).

[14] I.S. Kim, Y.T. Kim, S.I. Kim, I.H. Choi, Effects of hydrogen annealing on the electrical properties of $SrBi_2Nb_2O_9$ thin films, J. Korean Phys. Soc. 43 (2003) 850–853.

[15] J. Im, O. Acuciello, A.R. Krauss, D.M. Gruen, R.P.H. Chang, S.H. Kim, A.I. Kingon, Studies of hydrogen-induced degradation processes in $SrBi_2Ta_2O_9$ ferroelectric film-based capacitors, Appl. Phys. Lett. 74 (1999) 1162–1164.

[16] J. Thery, C. Dubourdieu, T. Baron, C. Ternon, H. Roussel, F. Pierre, MOCVD of $BiFeO_3$ thin films on $SrTiO_3$, Chem. Vap. Deposition 13 (2007) 232–238.

[17] S.G. Wang, G. Han, G.H. Yu, Y. Jiang, C. Wang, A. Kohn, R.C.C. Ward, Evidence for FeO formation at the Fe/MgO interface in epitaxial TMR structure by X-ray photoelectron spectroscopy, J. Magn. Magn. Mater. 310 (2007) 1935–1936.

[18] Y.C. Liang, Y.C. Liang, Nanoscale electrical and crystallographic properties of ultra-thin dielectric films, Thin Solid Films 518 (2010) S17–S21.

[19] J. Dho, X. Qi, H. Kim, J.L. MacManus-Driscoll, M.G. Blamire, Large electric polarization and exchange bias in multiferroic $BiFeO_3$, Adv. Mater. 18 (2006) 1445–1448.

[20] D. Hadad, T.-S. Chen, V. Balu, B. Jiang, S.H. Kuah, P. McIntyre, S. Summerfelt, J.M. Anthony, J.C. Lee, The effects of forming gas anneal on the electrical characteristics of ir-electroded BST thin film capacitors, Integr. Ferroelectr. 17 (1997) 461–469.

[21] P.C. McIntyre, J.H. Ahn, R.J. Becker, R.V. Wang, S.R. Gilbert, L.W. Mirkarimi, M.T. Schulberg, Deuterium in (Ba Sr)TiO_3 thin films: kinetics and mechanisms of incorporation and removal during annealing, J. Appl. Phys. 89 (2001) 6378–6389.

[22] C. Wang, M. Takahashi, H. Fujino, X. Zhao, E. Kume, T. Horiuchi, S. Sakai, Leakage current of multiferroic ($Bi_{0.6}Tb_{0.3}La_{0.1}$)FeO_3 thin films grown at various oxygen pressures by pulsed laser deposition and annealing effect, J. Appl. Phys. 99 (2006) 054104–054108.